CANCER BIOMARKERS

Mismatch repair deficiency predicts response of solid tumors to PD-1 blockade

Dung T. Le,[1,2,3] Jennifer N. Durham,[1,2,3]* Kellie N. Smith,[1,3]* Hao Wang,[3]* Bjarne R. Bartlett,[2,4]* Laveet K. Aulakh,[2,4] Steve Lu,[2,4] Holly Kemberling,[3] Cara Wilt,[3] Brandon S. Luber,[3] Fay Wong,[2,4] Nilofer S. Azad,[1,3] Agnieszka A. Rucki,[1,3] Dan Laheru,[3] Ross Donehower,[3] Atif Zaheer,[5] George A. Fisher,[6] Todd S. Crocenzi,[7] James J. Lee,[8] Tim F. Greten,[9] Austin G. Duffy,[9] Kristen K. Ciombor,[10] Aleksandra D. Eyring,[11] Bao H. Lam,[11] Andrew Joe,[11] S. Peter Kang,[11] Matthias Holdhoff,[3] Ludmila Danilova,[1,3] Leslie Cope,[1,3] Christian Meyer,[3] Shibin Zhou,[1,3,4] Richard M. Goldberg,[12] Deborah K. Armstrong,[3] Katherine M. Bever,[3] Amanda N. Fader,[13] Janis Taube,[1,3] Franck Housseau,[1,3] David Spetzler,[14] Nianqing Xiao,[14] Drew M. Pardoll,[1,3] Nickolas Papadopoulos,[3,4] Kenneth W. Kinzler,[3,4] James R. Eshleman,[15] Bert Vogelstein,[1,3,4] Robert A. Anders,[1,3,15] Luis A. Diaz Jr.[1,2,3]†‡

The genomes of cancers deficient in mismatch repair contain exceptionally high numbers of somatic mutations. In a proof-of-concept study, we previously showed that colorectal cancers with mismatch repair deficiency were sensitive to immune checkpoint blockade with antibodies to programmed death receptor–1 (PD-1). We have now expanded this study to evaluate the efficacy of PD-1 blockade in patients with advanced mismatch repair–deficient cancers across 12 different tumor types. Objective radiographic responses were observed in 53% of patients, and complete responses were achieved in 21% of patients. Responses were durable, with median progression-free survival and overall survival still not reached. Functional analysis in a responding patient demonstrated rapid in vivo expansion of neoantigen-specific T cell clones that were reactive to mutant neopeptides found in the tumor. These data support the hypothesis that the large proportion of mutant neoantigens in mismatch repair–deficient cancers make them sensitive to immune checkpoint blockade, regardless of the cancers' tissue of origin.

Therapy with immune checkpoint inhibitors has uncovered a subset of tumors that are highly responsive to an endogenous adaptive immune response (*1*). When the interaction between the checkpoint ligands and their cognate receptors on the effector cells is blocked, a potent and durable antitumor response can be observed, and on occasion this response can be accompanied by severe autoimmunity (*2–5*). These findings support the notion that many cancer patients contain in their immune system the capacity to react selectively to their tumors, ostensibly through recognition of tumor-specific antigens.

The molecular determinants that define this subset of tumors are still unclear; however, several markers, including PD-1 ligand (PD-L1) expression, RNA expression signatures, mutational burden, and lymphocytic infiltrates, have been evaluated in specific tumor types (*6–10*). Although such markers appear to be helpful in predicting response in specific tumor types, none of them have been evaluated prospectively as a pan-tumor biomarker. Another potential determinant of response is mutation-associated neoantigens (MANAs) that are encoded by cancers (*11–14*). Mismatch repair–deficient cancers are predicted to have a very large number of MANAs that might be recognized by the immune system (*15–18*). This prediction led us to conduct a small phase 2 study, focused on 11 patients with colorectal cancers, which demonstrated that PD-1 blockade was an effective treatment for many patients with these tumors (*19*). Since the initiation of that trial, other studies have shown that the number of mutations in mismatch repair–deficient colorectal cancers correlates with the response to PD-1 blockade, providing further support for a relationship between mutation burden and treatment response (*20*).

The genomes of mismatch repair–deficient tumors all harbor hundreds to thousands of somatic mutations, regardless of their cell of origin. We therefore sought to investigate the effects of PD-1 blockade (by the anti–PD-1 antibody pembrolizumab) in mismatch repair–deficient tumors independent of the tissue of origin. In the current study, we prospectively evaluated the efficacy of PD-1 blockade in a range of different subtypes of mismatch repair–deficient cancers (ClinicalTrials.gov number NCT01876511).

Eighty-six consecutive patients were enrolled between September 2013 and September 2016 (table S1). The data cutoff was 19 December 2016. All patients received at least one prior therapy and had evidence of progressive disease prior to enrollment. Twelve different cancer types were enrolled in the study (Fig. 1). All enrolled patients had evidence of mismatch repair deficiency as assessed by either polymerase chain reaction or immunohistochemistry. For most cases, germline sequencing of *MSH2*, *MSH6*, *PMS2*, and *MLH1* was performed to determine whether the mismatch repair deficiencies were associated with a germline change in one of these genes (i.e., whether the patients had Lynch syndrome) (table S2). Germline sequence changes diagnostic of Lynch syndrome were noted in 32 cases (48%), with *MSH2* being the most commonly mutated gene. In seven additional cases where germline testing was not performed, the patient reported a family history consistent with a diagnosis of Lynch syndrome.

Adverse events during treatment were manageable and resembled those found in other clinical studies using pembrolizumab (table S3). Although 74% of patients experienced an adverse effect, most were low-grade. Endocrine disorders, mostly hypothyroidism, occurred in 21% of patients and were easily managed with thyroid hormone replacement.

Seventy-eight patients had disease that could be evaluated by Response Evaluation Criteria in Solid Tumors (RECIST) (Table 1). Objective radiographic responses were noted in 46 of the 86 patients [53%; 95% confidence interval (CI), 42 to 64%], with 21% (n = 18) achieving a complete radiographic response. Disease control (measured as partial response + complete response + stable disease) was achieved in 66 of the 86 patients (77%; 95% CI, 66 to 85%). Radiographic responses could be separated into two classes. First, in 12 cases, scans at 20 weeks showed stable disease, which eventually converted to an objective response (measured as tumor size reduction in response to therapy, according to RECIST criteria). Second, in 11 additional cases, we observed

[1]Bloomberg-Kimmel Institute for Cancer Immunotherapy at Johns Hopkins, Baltimore, MD 21287, USA. [2]Swim Across America Laboratory at Johns Hopkins, Baltimore, MD 21287, USA. [3]Sidney Kimmel Comprehensive Cancer Center at Johns Hopkins, Baltimore, MD 21287, USA. [4]Ludwig Center and Howard Hughes Medical Institute at Johns Hopkins, Baltimore, MD 21287, USA. [5]Department of Radiology, Johns Hopkins University School of Medicine, Baltimore, MD 21287, USA. [6]Department of Medicine, Stanford University School of Medicine, Stanford, CA 94305, USA. [7]Providence Cancer Center at Providence Health & Services, Portland, OR 97213, USA. [8]Department of Medicine, University of Pittsburgh Cancer Institute, University of Pittsburgh School of Medicine, Pittsburgh, PA 15232, USA. [9]Gastrointestinal Malignancies Section, Thoracic-GI Oncology Branch, Center for Cancer Research, National Cancer Institute, Bethesda, MD 20892, USA. [10]Division of Medical Oncology, Ohio State University Comprehensive Cancer Center, Columbus, OH 43210, USA. [11]Merck & Co. Inc., Kenilworth, NJ 07033, USA. [12]West Virginia University Cancer Institute, Morgantown, WV 26506, USA. [13]Department of Gynecology and Obstetrics, Johns Hopkins Medicine, Baltimore, MD 21287, USA. [14]Caris Life Sciences, Phoenix, AZ 85040, USA. [15]Department of Pathology, Johns Hopkins University School of Medicine, Baltimore, MD 21287, USA.
*These authors contributed equally to this work. †Present address: Division of Solid Tumor Oncology, Memorial Sloan Kettering Cancer Center, New York, NY 10065, USA.
‡Corresponding author. Email: ldiaz@mskcc.org

Downloaded from https://www.science.org on September 19, 2024

JHU 2118
Merck Sharp v. Johns Hopkins
IPR2024-00649

an initial partial response or stable disease at the 20-week scan that later converted to a complete response while treatment was continued. The average time to any response was 21 weeks; the average time to complete response was 42 weeks (Fig. 1). Of note, the objective response rate was similar between colorectal cancer and other cancer subtypes. Specifically, we observed objective responses in 52% (95% CI, 36 to 68%) of patients with colorectal cancers and in 54% (95% CI, 39 to 69%) of the patients with cancers originating in other organs (tables S4 and S5). There was also no significant difference in the objective response rate between Lynch syndrome–associated and non–Lynch syndrome–associated tumors [46% (95% CI, 30 to 63%) versus 59% (95% CI, 41 to 76%), respectively; $P = 0.27$].

Neither median progression-free survival (PFS) nor median overall survival (OS) has yet been reached (median follow-up time of 12.5 months; Fig. 1), and the study is ongoing. However, the estimates of PFS at 1 and 2 years were 64% and 53%, respectively. The estimates of OS at 1 and 2 years were 76% and 64%, respectively, which is markedly higher than expected considering the advanced state of disease in this cohort (*21*). The PFS and OS were not significantly different in patients with colorectal cancers relative to those with other cancer types (fig. S1). Neither PFS [hazard ratio (HR) = 1.2 (95% CI, 0.582 to 2.512); $P = 0.61$] or OS [HR = 1.71 (95% CI, 0.697 to 4.196); $P = 0.24$] were influenced by tumors associated with Lynch syndrome.

Eleven patients achieved a complete response and were taken off therapy after 2 years of treatment. No evidence of cancer recurrence has been observed in those patients with an average time off therapy of 8.3 months. Seven other patients had residual disease by imaging, but pembrolizumab was discontinued after reaching the 2-year milestone or because of intolerance to therapy. To date, the average time off

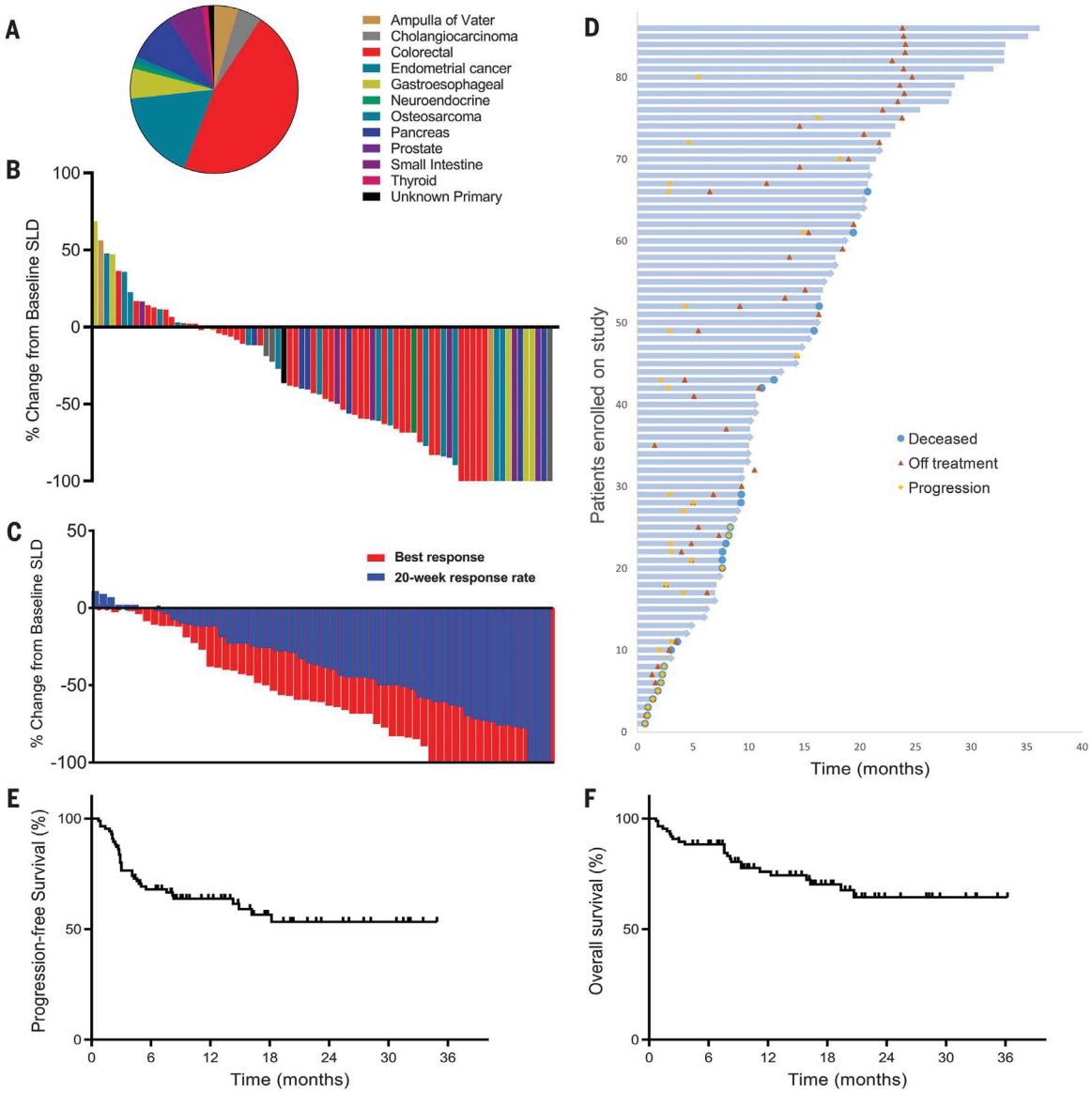

Fig. 1. Patient survival and clinical response to pembrolizumab across 12 different tumor types with mismatch repair deficiency. (**A**) Tumor types across 86 patients. (**B**) Waterfall plot of all radiographic responses across 12 different tumor types at 20 weeks. Tumor responses were measured at regular intervals; values show the best fractional change of the sum of longest diameters (SLD) from the baseline measurements of each measurable tumor. (**C**) Confirmed radiographic objective responses at 20 weeks (blue) compared to the best radiographic responses in the same patients (red). The mean time to the best radiographic response was 28 weeks. (**D**) Swimmer plot showing survival for each patient with mismatch repair–deficient tumors, indicating death, progression, and time off therapy. (**E** and **F**) Kaplan-Meier estimates of progression-free survival (E) and overall patient survival (F).

Downloaded from https://www.science.org on September 19, 2024

Table 1. Summary of therapeutic response to pembrolizumab (anti–PD-1) treatment. Radiographic responses, progression-free survival (PFS), and overall survival (OS) estimates were measured using RECIST v1.1 guidelines. Patients were considered not evaluable if clinical progression precluded a 12-week scan. The rate of disease control was defined as the percentage of patients who had a complete response, partial response, or stable disease for 12 weeks or more. NR, not reached.

Type of response	Patients (*n* = 86)
Complete response	18 (21%)
Partial response	28 (33%)
Stable disease	20 (23%)
Progressive disease	12 (14%)
Not evaluable	8 (9%)
Objective response rate	53%
95% CI	42 to 64%
Disease control rate	77%
95% CI	66 to 85%
Median progression-free survival time	NR
95% CI	14.8 months to NR
2-year progression-free survival rate	53%
95% CI	42 to 68%
Median overall survival time	NR
95% CI	NR to NR
2-year overall survival rate	64%
95% CI	53 to 78%

therapy for this group was 7.6 months. As of the data cutoff, none of these patients has shown evidence of progression since discontinuation of pembrolizumab.

Twenty patients with measurable radiographic disease underwent percutaneous biopsies between 1 month and 5 months after the initiation of therapy. Twelve of these biopsies demonstrated no evidence of tumor cells and were shown to have varying degrees of inflammation, fibrosis, and mucin, consistent with an ongoing immune response (fig. S2). The other eight cases showed residual tumor cells. The absence of cancer cells in posttreatment biopsies was a strong predictor of PFS [HR for PFS = 0.189 (95% CI, 0.046 to 0.767); $P = 0.012$], with median PFS of 25.9 months versus 2.9 months for biopsies with evidence of residual tumor. Although there was no significant difference in OS between patients whose biopsies were positive or negative for tumor cells, median OS has not yet been reached in patients with negative biopsies (table S6).

Primary clinical resistance to initial therapy with pembrolizumab, as measured by progressive radiographic disease on the first study scan, was noted in 12 patients (14%) (Table 1). After determining the exomic sequences of tumor and matched normal DNA from three of these patients, we compared them to the exomes of 15 primary tumors from patients who had achieved objective responses to the therapy (table S7). The three therapy-insensitive tumors harbored an average of 1413 nonsynonymous mutations, not significantly different from the number in patients with objective responses (1644 nonsynonymous mutations; $P = 0.67$, Student *t* test). The gene (*B2M*) encoding β_2-microglobulin, a protein required for antigen presentation (*22*), was not mutated in any of the primary tumors from the resistant group (table S8).

Only five cases of acquired resistance were noted, where patients developed progressive disease after an initial objective response to pembrolizumab. Three of these cases were atypical in that the tumors emerged in occult sites such as the brain (two cases) or bone (one case). All three cases were treated with local therapy (radiation or surgery), and the patients survived and continued treatment with pembrolizumab. However, in accordance with study design, these three patients are listed in Fig. 1 as having progressive disease.

We performed exome sequencing of biopsies of brain metastases from two patients and compared the results with those of their primary tumors (fig. S3 and table S7). In the first case, the primary duodenal tumor and brain metastasis shared 397 nonsynonymous somatic mutations, providing unequivocal evidence that the metastasis was derived from the primary duodenal tumor rather than from an independent tumor. Moreover, the metastasis harbored 1010 nonsynonymous new mutations not present in the primary tumor, while the primary tumor harbored 964 mutations not present in the metastasis (table S9). In the second case, the primary colorectal tumor and brain metastasis shared 848 nonsynonymous somatic mutations, similarly providing unequivocal evidence of a genetic relationship between the two lesions. The brain metastasis harbored 221 nonsynonymous mutations not present in the primary colorectal tumor, while the primary tumor harbored 100 mutations not present in the metastasis (table S10). Of note, the brain metastases from both of these patients contained mutations in the *B2M* gene. In the patient with the colorectal tumor, a truncating mutation (L15Ffs*41) in the *B2M* gene was identified in the metastasis but not in the primary tumor. The primary duodenal tumor harbored a truncating mutation in β_2-microglobulin (V69Wfs*34), whereas the metastasis retained this mutation and acquired a second *B2M* mutation (12L>P; table S7).

We also evaluated the exomes of three primary tumors from patients who originally had stable disease by RECIST criteria at 20 weeks, but whose disease progressed within 8 months of initiating therapy. The average mutational burden was 1647 for this group, similar to those of the other patients described above. Interestingly, two of these three tumors harbored mutations of *B2M* (table S7).

We next sought to directly test the hypothesis that checkpoint blockade induces peripheral expansion of tumor-specific T cells and that mismatch repair–deficient tumors harbor functional MANA-specific T cells. Deep sequencing of T cell receptor CDR3 regions (TCR-seq) has emerged as a valuable technique to evaluate T cell clonal representation in both tumors and peripheral blood. We performed TCR-seq on tumors from three responding patients (obtained from archival surgical resections) and identified intratumoral clones that were selectively expanded in the periphery (Fig. 2A). These clones were present at very low frequency (often undetectable) in the peripheral blood before pembrolizumab treatment, but many rapidly increased after treatment initiation, followed by a contraction that generally occurred before radiologic responses were observed. To characterize functional T cell clones specific for mutant peptides, we obtained peripheral blood from one of the patients (subject 19). We tested the patient's posttreatment peripheral blood for reactivity against the 15 top candidate MANAs as identified via a neoantigen prediction algorithm [specified by the patient's human leukocyte antigen (HLA) class I alleles; see supplementary materials] with an interferon-γ (IFN-γ) ELISpot assay. Counts of spot-forming cells or cytokine activity analyses revealed T cell responses against 7 of 15 peptides (Fig. 2, B and C). We next interrogated the expanded lymphocyte populations against these seven peptides with TCR-seq. Clonal T cell expansion was noted in response to three of the seven peptides (Fig. 2D), with specificity demonstrated by a lack of expansion in response to any other peptide tested (fig. S4). In the peripheral blood, T cell expansion to these three mutant peptides resulted in 142 unique TCR sequences, seven of which were found in the tumor sample (two from MANA1, three from MANA2, and two from MANA4) (Fig. 2D). Of note, the mutant peptides that scored positive all resulted from frameshift mutations—the type of mutation that is most characteristic of mismatch repair–deficient cancers.

All seven of the MANA-reactive TCRs were detectable in peripheral blood at very low frequency (less than 0.02%) before treatment. However, four of the clones rapidly increased in frequency in the peripheral blood after anti–PD-1 treatment (Fig. 2E). Similar to results from the three patients

Downloaded from https://www.science.org on September 19, 2024

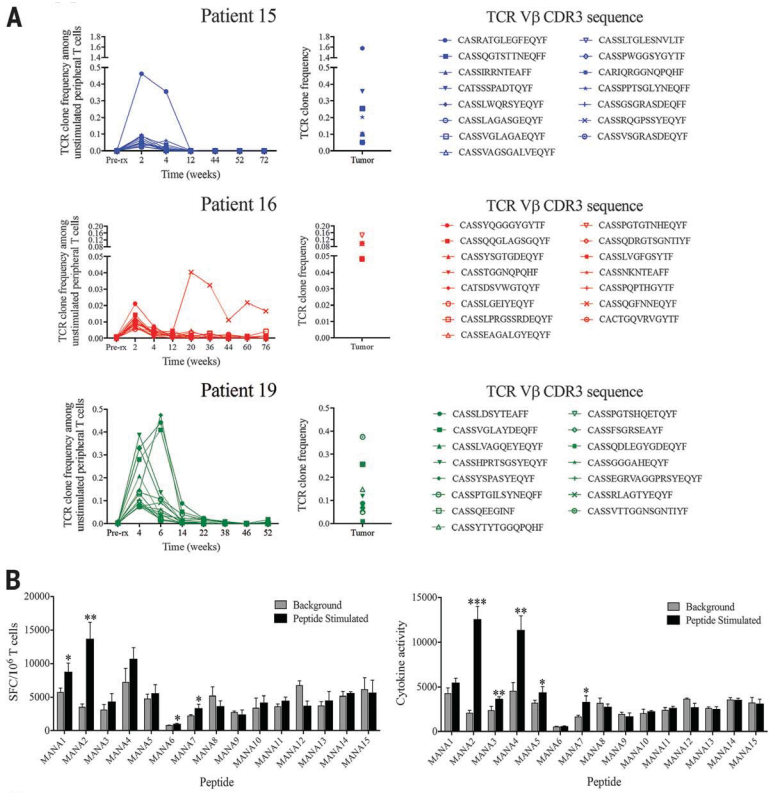

C

Candidate MANAs	Gene	Mutation	Mutation type	Consequence	Mutant peptide	MHC class I restriction	Predicted mutant IC50 (nM)	WT peptide	Predicted WT IC50 (nM)
MANA1	BTBD7	Y324Ifs*22	ins	Frameshift	NSDITLYVY	HLA-A*01:01	6.7	NA	NA
MANA2	SLC16A4	F475Lfs*12	del	Frameshift	LSSVSFFLY	HLA-A*01:01	16.5	LSSVSFFFV	2245.1
MANA3	CLPP	A10Pfs*117	del	Frameshift	RSFPSWWSR	HLA-A*31:01	4.4	NA	NA
MANA4	DEPDC1	K418Rfs*45	del	Frameshift	SLMSKKFLPL	HLA-B*08:01	10.3	NA	NA
MANA5	HAND2	32A>-	del	In-frame deletion	MALSYSPEY	HLA-B*35:01	2.0	SMALSYSPE	22,533.8
MANA6	ITPR2	K343Nfs*27	del	Frameshift	MAMTLHPF	HLA-B*35:01	2.7	NA	NA
MANA7	SHANK3	G227Vfs*15	del	Frameshift	MPSAVSCF	HLA-B*35:01	2.7	NA	NA

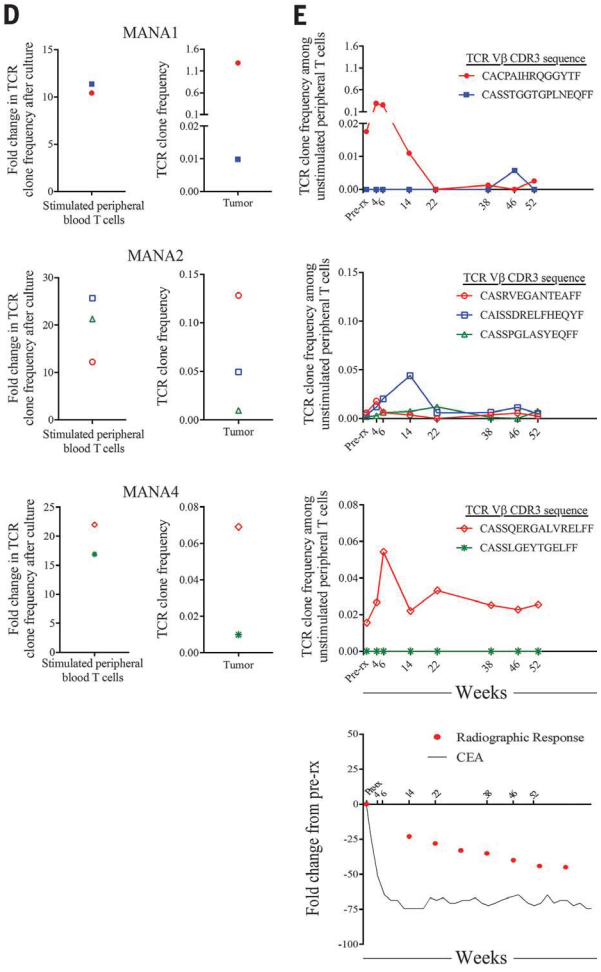

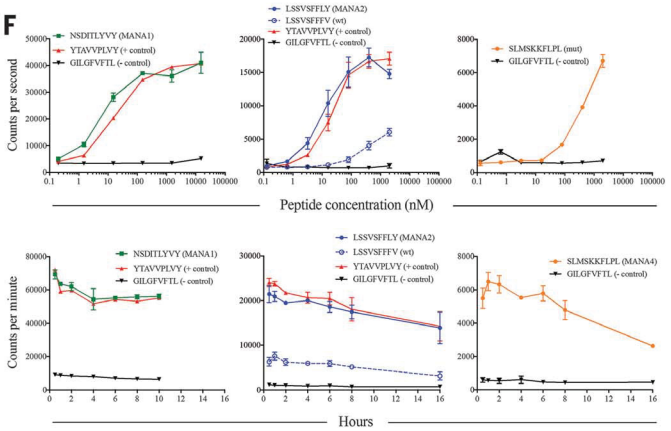

Fig. 2. TCR clonal dynamics and mutation-associated neoantigen recognition in patients responding to PD-1 blockade. (**A**) TCR sequencing was performed on serial peripheral T cell samples obtained before and after PD-1 blockade. Tumor tissue with mismatch repair deficiency was obtained from three responding patients. Shown for each patient are 15 TCR clones with the highest relative change in frequency after treatment (left) that were also found in the original tumor (right panels). (**B**) Whole-exome sequencing was performed on tumor and matched normal tissue from patient 19. Somatic alterations were analyzed using a neoantigen prediction pipeline to identify putative MANAs. Reactivity to 15 candidate MANAs was tested in a 10-day cultured IFN-γ ELISpot assay. Data are shown as the mean number of spot-forming cells (SFC) per 10^6 T cells (left) or mean cytokine activity (right) of triplicate wells ± SD. $*P < 0.05$, $**P < 0.01$, $***P < 0.001$. (**C**) Seven candidate MANAs were selected for TCR analysis on the basis of ELISpot reactivity. (**D**) MANA-specific T cell responses were identified against three of seven candidate MANAs (MANA1, MANA2, and MANA4) after 10 days of in vitro stimulation (left panels). MANA-specific clones were identified by significant expansion in response to the relevant peptide and no significant expansion in response to any other peptide tested (fig. S3). Data are shown as the relative change in TCR clone frequency compared to the frequency of that clone after identical culture without peptide. These T cell clones were also found in the original tumor biopsy (right panels). (**E**) Frequency of MANA-specific clones, carcinoembryonic antigen (CEA), and radiographic response in the tumor [from (D)] were tracked in the peripheral blood before treatment and at various times after pembrolizumab treatment. Time is shown in weeks after the first pembrolizumab dose. (**F**) In vitro binding and stability assays demonstrate the affinity kinetics of each relevant MANA and the corresponding wild-type peptide (when applicable) for their restricting HLA class I allele. The A*02:01-restricted influenza M GILGFVTL epitope was used as a negative control for each assay; known HLA-matched epitopes were used as positive controls when available. Data are shown as counts per second with increasing peptide concentration for binding assays (top) or counts per minute over time for stability assays (bottom). Data points indicate the mean of two independent experiments ± SD. Amino acid abbreviations: A, Ala; C, Cys; D, Asp; E, Glu; F, Phe; G, Gly; H, His; I, Ile; K, Lys; L, Leu; M, Met; N, Asn; P, Pro; Q, Gln; R, Arg; S, Ser; T, Thr; V, Val; W, Trp; Y, Tyr.

Downloaded from https://www.science.org on September 19, 2024

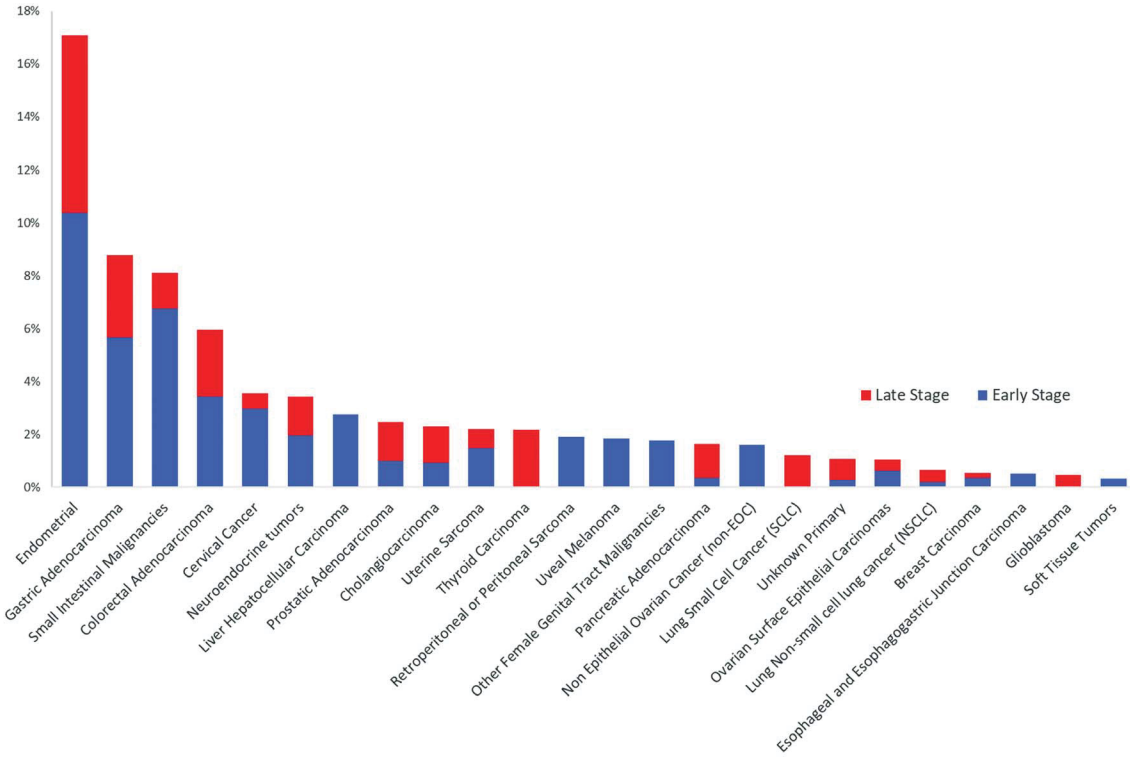

Fig. 3. Mismatch repair deficiency across 12,019 tumors. The proportion of mismatch repair–deficient tumors in each cancer subtype is expressed as a percentage. Mismatch repair–deficient tumors were identified in 24 of 32 tumor subtypes tested, more often in early-stage disease (defined as stage < IV).

analyzed above, the frequencies of these functionally validated MANA-specific T cell clones peaked soon after treatment and corresponded with normalization of the systemic tumor marker, predating objective radiographic response by several weeks. This peak in T cell clonal expansion was followed by decreases in frequency, reminiscent of T cell responses to acute viral infections (Fig. 2E). Because all the MANAs were from frameshift mutations, only MANA2 had a similar wild-type counterpart (differing in the two C-terminal amino acids). The corresponding wild-type peptide bound to HLA with less than 1% of the affinity of the mutant peptide counterpart (Fig. 2F), consistent with the mutation conferring enhanced HLA binding.

To estimate the proportion of cancer patients for whom the results of this study might be applicable, we evaluated 12,019 cancers representing 32 distinct tumor types for mismatch repair deficiency using a next-generation sequencing–based approach (Fig. 3). In accordance with a recent independent estimate using a different approach (*23*), we found that >2% of adenocarcinomas of the endometrium, stomach, small intestine, colon and rectum, cervix, prostate, bile duct, and liver, as well as neuroendocrine tumors, uterine sarcomas, and thyroid carcinomas, were mismatch repair–deficient. Across these 11 tumor types, 10% of stage I to stage III cancers and 5% of stage IV cancers were mismatch repair–deficient. This represents roughly 40,000 annual stage I to III diagnoses and 20,000 stage IV diagnoses in the United States alone. Because genetic and immunohistochemical tests for mismatch repair deficiency are already widely available, these results tie immunity, cancer genetics, and therapeutics together in a manner that will likely establish a new standard of care. In the future, testing for mismatch repair deficiency in patients who are refractory to other treatments might be considered in order to identify those who may benefit from PD-1 pathway blockade, regardless of tumor type.

REFERENCES AND NOTES

1. S. L. Topalian, C. G. Drake, D. M. Pardoll, *Cancer Cell* **27**, 450–461 (2015).
2. P. C. Tumeh *et al.*, *Nature* **515**, 568–571 (2014).
3. D. F. McDermott *et al.*, *J. Clin. Oncol.* **33**, 2013–2020 (2015).
4. S. L. Topalian *et al.*, *J. Clin. Oncol.* **32**, 1020–1030 (2014).
5. S. N. Gettinger *et al.*, *J. Clin. Oncol.* **33**, 2004–2012 (2015).
6. J. M. Taube *et al.*, *Clin. Cancer Res.* **20**, 5064–5074 (2014).
7. N. J. Llosa *et al.*, *Cancer Discov.* **5**, 43–51 (2015).
8. R. S. Herbst *et al.*, *Nature* **515**, 563–567 (2014).
9. N. A. Rizvi *et al.*, *Science* **348**, 124–128 (2015).
10. W. Hugo *et al.*, *Cell* **168**, 542 (2017).
11. N. H. Segal *et al.*, *Cancer Res.* **68**, 889–892 (2008).
12. M. M. Gubin *et al.*, *Nature* **515**, 577–581 (2014).
13. T. N. Schumacher, R. D. Schreiber, *Science* **348**, 69–74 (2015).
14. J. P. Ward, M. M. Gubin, R. D. Schreiber, *Adv. Immunol.* **130**, 25–74 (2016).
15. C. Lengauer, K. W. Kinzler, B. Vogelstein, *Nature* **396**, 643–649 (1998).
16. H. Kim, J. Jen, B. Vogelstein, S. R. Hamilton, *Am. J. Pathol.* **145**, 148–156 (1994).
17. T. C. Smyrk, P. Watson, K. Kaul, H. T. Lynch, *Cancer* **91**, 2417–2422 (2001).
18. R. Dolcetti *et al.*, *Am. J. Pathol.* **154**, 1805–1813 (1999).
19. D. T. Le *et al.*, *N. Engl. J. Med.* **372**, 2509–2520 (2015).
20. M. Overman *et al.*, *J. Clin. Oncol.* **35** (suppl.), 519 (2017).
21. A. Grothey *et al.*, *Lancet* **381**, 303–312 (2013).
22. J. M. Zaretsky *et al.*, *N. Engl. J. Med.* **375**, 819–829 (2016).
23. R. J. Hause, C. C. Pritchard, J. Shendure, S. J. Salipante, *Nat. Med.* **22**, 1342–1350 (2016).

ACKNOWLEDGMENTS

The data reported are tabulated in the main text and supplementary materials. The raw TCR RNA sequence data have been deposited into the ImmuneACCESS project repository of the Adaptive Biotech database, under the following link: https://clients.adaptivebiotech.com/pub/diaz-2017-science. We thank K. Helwig for administrative support, C. Blair for outstanding technical assistance, and E. H. Rubin, R. Dansey, and R. Perlmutter at Merck & Co. Inc. (Kenilworth, NJ) for supporting this research. Funded by the Swim Across America Laboratory at Johns Hopkins, the Ludwig Center for Cancer Genetics and Therapeutics, the Howard Hughes Medical Institutes, the Bloomberg-Kimmel Institute for Cancer Immunotherapy at Johns Hopkins, the 2017 Stand Up to Cancer Colon Cancer Dream Team, the Commonwealth Fund, the Banyan Gate Foundation, the Lustgarten Foundation for Pancreatic Cancer Research, the Bloomberg Foundation, the Sol Goldman Pancreatic Cancer Research Center, Merck & Co. Inc., Gastrointestinal SPORE grant P50CA062924, and NIH grants P30CA006973, CA163672, CA43460, CA203891, CA67941, CA16058, and CA57345. L.D., D.L., B.V., N.P., and K.W.K. are inventors on a patent application (PCT/US2015/060331 or WO 2016077553 A1) submitted by Johns Hopkins University that covers checkpoint blockade and microsatellite instability. L.D., B.V., N.P., and K.W.K. are founders of PapGene and Personal Genome Diagnostics (PGDx). L.D. is a consultant for Merck, Illumina, PGDx, and Cell Design Labs. PGDx and PapGene, as well as other companies, have licensed technologies from Johns Hopkins University, on which L.D., B.V., N.P., and K.W.K. are inventors. Some of these licenses and relationships are associated with equity or royalty payments. The terms of these arrangements are being managed by Johns Hopkins and Memorial Sloan Kettering in accordance with its conflict-of-interest policies.

SUPPLEMENTARY MATERIALS

www.sciencemag.org/content/357/6349/409/suppl/DC1
Materials and Methods
Figs. S1 to S4
Tables S1 to S10
References (*24*–*36*)

17 May 2017; accepted 1 June 2017
Published online 8 June 2017
10.1126/science.aan6733

Downloaded from https://www.science.org on September 19, 2024